Crystal field properties of f-electron states in $RBa_2Cu_3O_7$ for R=Ho, Nd and Pr

1991 J. Phys.: Condens. Matter 3 49

(http://iopscience.iop.org/0953-8984/3/1/004)

J. Phys.: Condens. Matter 3 (1991) 49–67. Printed in the UK

Crystal-field properties of f-electron states in $RBa_2Cu_3O_7$ for R = Ho, Nd and Pr

G L Goodman, C-K Loong and L Soderholm
Argonne National Laboratory, Argonne, IL 60439, USA

Received 19 June 1990, in final form 4 September 1990

Abstract. We present details of our predictions for the crystal-field-split levels in $RBa_2Cu_3O_7$ compounds with $R = Nd^{3+}$ ($f^3\ ^4I_{9/2}$) and Pr^{3+} ($f^2\ ^3H_4$) based on the previously reported crystal-field split energy levels of $f^{10}\ ^5I_8$ for Ho^{3+} in $HoBa_2Cu_3O_7$. Our predictions of the overall distribution of crystal-field levels provide the framework for interpretation of inelastic neutron scattering spectra of $NdBa_2Cu_3O_7$ and $PrBa_2Cu_3O_7$. For $NdBa_2Cu_3O_7$ the inelastic scattering peaks are clearly seen and can be well assigned in terms of the energy levels of $f^3\ ^4I_{9/2}$ by a small re-scaling of the predicted crystal-field parameters to adjust the overall width of the calculated spectrum. In the case of $PrBa_2Cu_3O_7$ several important inelastic scattering features, particularly the lowest energy ones, are so unusually broad and weak that it was difficult to identify them without predictions of this type. Enough features in the scattering spectra have now been assigned for us to obtain fitted values for the crystal-field parameters of Pr^{3+} and Nd^{3+} in $RBa_2Cu_3O_7$. As tests of these new assignments we discuss predictions of the anisotropies of magnetic susceptibility and the thermodynamic functions for the paramagnetic phase of $PrBa_2Cu_3O_7$. Finally, a primitive model for interactions between Pr^{3+} ions is used to give an initial interpretation of the saturation moment that has been reported for the antiferromagnetically ordered phase of $PrBa_2Cu_3O_7$. We conclude that standard crystal-field theory correctly applied to the f^2 configuration of the Pr^{3+} ions fully explains the unusual magnetic properties of $PrBa_2Cu_3O_7$.

1. Introduction

In our experimental paper [1] (referred to here as I), magnetic susceptibility and neutron scattering studies of $RBa_2Cu_3O_7$ ($R123O_7$) for R = Ho, Nd and/or Pr are presented. Unusual properties of the Pr compound and the relationship of its magnetic properties to the absence of superconductivity in this material have been discussed at length [1].

Our understanding of the magnetic and thermophysical properties for these $R123O_7$ materials depends crucially on knowledge of the electronic structure at low energies ($E < 100$ meV) along with the corresponding excitation energies for the rare earth, R. Experimentally, relatively little effort has been directed toward determining the f-electron energy level structure for the rare earth components in these materials, as compared to the efforts made to learn about the Fermi surface and other electronic properties. In part, this situation arises from a high absorption of light in the interesting energy range that creates experimental problems in obtaining optical spectra for $R123O_7$ materials. From a theoretical viewpoint, initial interest in the electronic properties of these materials has focused on the CuO planes and chains, where it is widely believed

0953-8984/91/010049 + 19 $03.50

that the superconducting carriers are located [2]. Two recent developments have created a need for more detailed information on the electronic properties of the rare earth R in $R123O_7$.

First, the non-superconducting behaviour of the R = Pr and Cm members of the series has focused interest on the electronic properties of R in a search concentrated on understanding what is different about these f-elements [3–5]. Although both these members are isostructural with the superconducting Y analogue ($YBa_2Cu_3O_7$), they are not superconducting. Recently it was proposed that the absence of superconductivity in these samples arises from an interaction between the magnetic f-electrons and the electrons in the CuO planes [4–6]. An understanding of this interaction seems essential to resolve the question of why these two f-electron elements have a profound influence on the superconductivity of the host materials, whilst other rare earths do not.

The second development to focus attention on the electronic properties of R in $R123O_7$ involves the coexistence of superconductivity and three-dimensional (3D) magnetic ordering of the R moments at low temperatures. Several of the R ions, including Pr, Nd, Gd, Dy, and Er, have been shown to exhibit long range 3D ordering of the f moments at low temperatures coexistent with the superconducting state [7]. An understanding of both the nature of the magnetic ordering and its apparent lack of influence on the superconducting critical temperature (T_c) requires a detailed understanding of the low-lying energy levels of R. The antiferromagnetic order of pure $Pr123O_7$ is particularly interesting by way of contrast to these cases of coexistence of superconductivity and magnetic ordering. Pure $Pr123O_7$ has an unusually high ordering temperature ($T_N \sim 17$ K) and a low value for its ordered moment, i.e. 0.74 μ_B, where μ_B is the Bohr magneton [8, 9]. The relation between these ordered-state properties and the absence of superconductivity for pure $Pr123O_7$ may be highly significant.

Inelastic neutron scattering (INS) is the best known method for direct measurements of the low-energy electronic excitation spectrum, particularly for optically opaque materials like $R123O_7$. However, interpretation of INS data for $R123O_7$ materials has been by no means straightforward. Although well defined crystal-field excitations have been observed in most of the $R123O_7$ magnetic high-T_c superconductors, acceptable assignments of the observed features to crystal-field split energy levels have been difficult to obtain, except perhaps in the case of $Ho123O_7$ [10]. In the case of non-superconducting pure $Pr123O_7$, the situation is even more complicated because INS measurements reveal no strong, well defined peaks up to ~200 meV. Given these difficulties in understanding the neutron scattering results and with the two aforementioned developments in mind, we have conducted a systematic study of the crystal-field level structure for f-electron states in the $R123O_7$ system for R = Nd, Pr and Ho.

Neutron inelastic spectra for $Nd123O_7$ at 15 K from the intense Pulsed Neutron Source (IPNS) located at Argonne National Laboratory are reported in I. Sharp crystal-field peaks have been observed at 12, 20.8, 36 and 117 meV. These peak energies agree well with those previously reported up to 40 meV [11, 12], except for a feature near 5.8 meV [12]. This feature is absent from our spectra of $Nd123O_7$ but appears in our spectra of $Nd_{1.5}Ba_{1.5}Cu_3O_7$. On the other hand, the small peak at 12 meV in figure 1 of paper I arises almost entirely from scattering of the Nd^{3+} ions in $Nd123O_7$ even though it occurs at just the same energy as another crystal-field excitation associated with disordered Nd ions residing at the Ba sites. No additional peaks in $Nd123O_7$ are observed up to about 200 meV.

Neutron inelastic scattering spectra observed for $Pr123O_7$ obtained at IPNS are presented in figure 2 of paper I. Additional IPNS data obtained at 15 and 25 K are reported

here in figure 1. A most noteworthy feature of all this data is the lack of any strong, sharp peaks. Instead we see an intense, broad component of magnetic excitation in the 15 K spectrum (figure 1(*a*)) from ~2 to ~10 meV and much weaker, broadened features in the 25 K spectrum (figure 1(*b*)) at about 35, 45, 50, 65, 80 and, perhaps, 105 meV. In our experimental paper, we present evidence and analysis based on several observations that the feature at 35 meV is not a magnetic scattering feature associated with the crystal-field energy levels [1]. Our results up to 110 meV are consistent with recent observations in similar experiments by Paul *et al* [13] at the ISIS facility of the Rutherford Appleton Laboratory.

According to a brief, preliminary report, about inelastic neutron scattering experiments on $Y123O_7$ and $Pr123O_7$ performed at ISIS, there is evidence at 2 K for five resolved, crystal-field peaks for $Pr123O_7$ at energies of 65, 85, 105, 113, and 123 meV [13]. These authors also state that there may be a sixth peak at about 130 meV. Like the data presented here and in paper I, their data show unusually broad features so that they speak of 'considerable intrinsic width of the peaks.' The data of Paul *et al* [13] show a significant feature near 35 meV in the $Y123O_7$ spectrum at 2 K that is consistent with our observations for $Y123O_7$ and with our assignment of the 35 meV feature for $Pr123O_7$ to a lattice mode [1]. Combining both sets of data, we find evidence for perhaps as many as ten crystal-field transitions associated with Pr in $Pr123O_7$ between 15 and 150 meV.

In addition to the aforementioned studies, magnetic neutron scattering data on energy transfer in the range 0–10 meV have been reported for $Pr123O_7$ with good statistics for both energy loss [12] and energy gain [14] by the scattering material. At 50 K a broad double-humped feature centred around 2.5 meV is found in both energy transfer regions. Both experimental groups were unable to make any definitive assignment of the features in their data because they were unsure of the number of crystal-field levels to expect in this energy range.

In the next section about crystal-field analysis we show that, based on the scaled crystal field from $Ho123O_7$, we expect to find two low-lying excited electronic states for $Pr123O_7$ in this energy range. When one knows to look for just two low-lying excited energy levels, interpretation of the data becomes straightforward. From the double-humped spectra one excited level can be assigned near 1.4 meV, and the other near 3.9 meV. Our assignments are shown in figure 2(*a*) for energy gain and figure 2(*b*) for energy loss. A 2.5 meV hot-band feature is produced by transitions connecting the excited levels at 1.4 and 3.9 meV. It is worth noting that the combined effects of thermal weighting and magnetic transition strengths make this hot-band feature an important component in both energy transfer spectra.

We have simulated these observed spectra by summing Lorentzian line shapes centred at the assigned energies with relative intensities proportional to the Boltzmann population factor times the transition strength calculated in section 2 from crystal-field analysis. The simulated spectra, as shown in figures 1 and 2, seem to give satisfactory representations of the observed, broad spectra. For powder samples, we use an equal average over each crystallographic direction for the effective transition strength. The full Lorentzian widths at half maximum (FWHM) are 3.9, 8.0 and 3.8 meV for figures 1(*a*), 1(*b*) and 2, respectively. The 3.9 and 8.0 meV widths for the scattering features in figure 1 are the root of the sum of squares of the appropriate instrumental widths, about 0.9 and 7 meV, respectively, and the intrinsic width for $Pr123O_7$, about 3.8 meV. On the other hand, only the intrinsic width is significant for the spectra in figure 2 because the instrumental width in these cases is about an order of magnitude smaller than the intrinsic width for each of the six scattering features of $Pr123O_7$ that are found in this

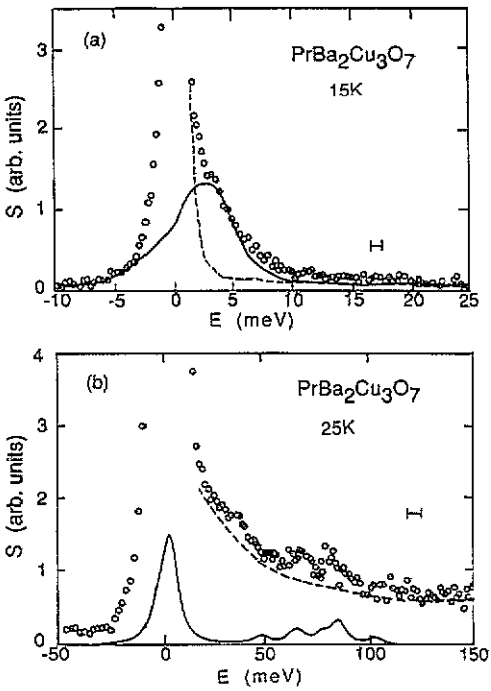

Figure 1. Measured scattering function S in arbitrary units for $PrBa_2Cu_3O_7$. The positive and negative energy scale represents crystal-field excitations and de-excitations, respectively. The broken curves represent estimated background due to phonon scattering in the same energy region. The instrumental energy resolution (FWHM) is indicated by horizontal bars. The simulated spectrum is based on Lorentzian line shapes with FWHM of 3.9 or 8.0 meV in (a) or (b), respectively, that combines the appropriate instrumental width of 0.9 or 7.0 meV with an intrinsic width of 3.8 meV for the features of $Pr123O_7$.

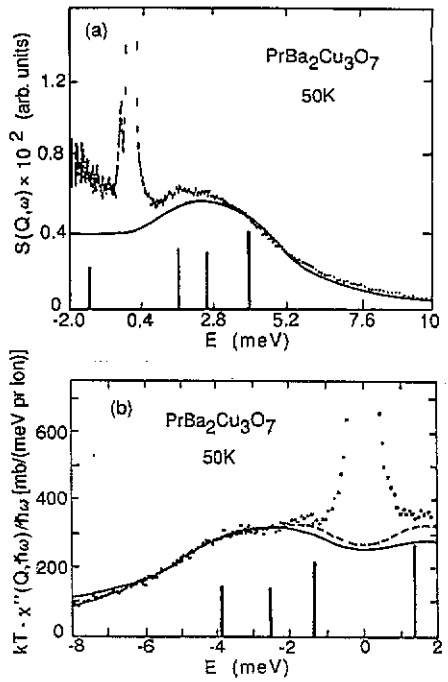

Figure 2. (a) Magnetic scattering for $PrBa_2Cu_3O_7$ at 50 K observed by inelastic neutron scattering ($S(Q, \omega)$ in arbitrary units), from figure 3 of [14]. (b) Background-corrected spectrum: the broken curve indicates the magnetic contribution, showing $kT\chi''/E = S(Q, \omega)[1 - \exp(-E/kT)]\, kT/E$, from figure 4 of [12]. In both (a) and (b) the positive and negative energy scale indicates crystal-field excitations and de-excitations, respectively. Positions and relative magnetic transition strengths for the assigned energy levels of $f^2\ ^3H_4$ for $PrBa_2Cu_3O_7$ have been shown by vertical bars. Simulated spectra are shown as full curves, based on Lorentzian line shapes with full width at half maximum of 3.8 meV.

energy-transfer region, i.e. between −8 and +10 meV. Thus, we believe that the spectra from the literature [12, 14] provide important information on the strength of interaction between individual Pr atoms and the rest of the atoms in $Pr123O_7$. We return to this point in our discussion of magnetic and thermodynamic properties in section 3.

Magnetic ordering of the Pr moments in $Pr123O_7$ occurs below 17 K [8, 9, 15]. The positions of the lowest energy levels for the Pr ions can be strongly effected by this type of magnetic ordering. We are trying to understand the properties of the $R123O_7$ materials in terms of the crystal-field split energy levels of the appropriate f^n configuration. Thus, it is important that we are basing our assignments for $Pr123O_7$ on energy-transfer spectra for samples at 25 and 50 K, well above the magnetic ordering temperature. In the next

section we work through the details of applying crystal-field theory to the $R123O_7$ compounds. In section 2 we also show that our newly assigned low-lying energy levels for $Pr123O_7$ are consistent with the crystal-field assignments for $Ho123O_7$ as given by Furrer *et al* [10].

Although much is known about the theory of crystal-fields in rare earth compounds (see for example the review by Fulde [16]) it is often difficult to know from what size crystal-field and free-ion parameters to start in making assignments of neutron scattering results for any particular material. In the case of $R123O_7$ we can use work of Furrer *et al* on $Ho123O_7$ to tell us about the appropriate size of the crystal field [10] and work of Carnall *et al* on lanthanide ions doped in LaF_3 to tell us about the appropriate free-ion parameters [17].

In the following section, we present details of scaling crystal-field parameters from one rare earth compound to analogous compounds of other rare earth ions. We use this technique to relate parameters for Ho^{3+}, Nd^{3+} and Pr^{3+}. These semi-empirical parameters are used to calculate transition energies and intensities leading to assignments of the observed crystal-field levels within the lowest-lying Russell–Saunders multiplet for the corresponding $R123O_7$ compounds. We have been able to give crystal-field assignments for $Nd123O_7$ and $Pr123O_7$, as well as new, slightly improved assignments for $Ho123O_7$. Magnetic susceptibilities have been calculated as a function of temperature for all three compounds. The calculated and experimental magnetic susceptibilities for powder samples have been shown to agree in paper I [1].

In the present paper, we are mainly concerned with two objectives. Firstly, to give a careful formulation of crystal field theory as it applies to the $R123O_7$ materials so that reliable energy-level assignments can be made for R = Nd and Pr and secondly, to make predictions for additional properties of $Pr123O_7$ that provide more rigorous tests of its electronic structure in our view. We base these predictions on crystal-field parameters for $Pr123O_7$ that are slightly revised from the values given in paper I. These new crystal-field parameters for $Pr123O_7$ are what can be called 'consensus' values obtained by analysing various experimental inelastic neutron scattering data in the literature.

In section 3 we discuss the predicted magnetic anisotropy and thermodynamic functions in the paramagnetic phase of this material. We make comparisons with available data on the specific heat of $Pr123O_7$. Experiments to measure the anisotropy of the magnetic susceptibility would be very helpful in confirming our symmetry assignments for the three lowest energy levels of $Pr123O_7$. We show that the low-temperature ordered moment found for $Pr123O_7$ [8] is consistent with our crystal-field analysis for Pr^{3+} ions. Thus we support the conclusion stressed in paper I that there is no need to invoke Pr^{4+} ions to explain the magnetic properties of $Pr123O_7$. Standard crystal-field theory correctly applied to Pr^{3+} ions fully explains neutron scattering and all other magnetic data for this unusual material in its paramagnetic phase.

2. Crystal-field analysis

We have extended the crystal-field computer programs developed for energy-level calculations by Crosswhite and Crosswhite [18] so that we can also calculate magnetic properties of the f^n configurations. The method that we use relies on two key assumptions. Firstly, that the f^n electronic states are well removed from other electronic states,

and secondly, that the crystalline electric field can be treated as a small perturbation of the f^n free-ion energy levels. The Hamiltonian used has the form

$$H = H_0 + H_{EL} + H_{SO} + H_{IN} + H_{CF}.$$

Here, H_0 is the spherically symmetric one-electron part of the Hamiltonian, involving the kinetic energy of the electrons and the central Coulomb field.

$$H_{EL} = \sum_{k=0,2,4,6} f_k F^k$$

and

$$H_{SO} = A_{SO}\zeta_f.$$

The adjustable parameters F^k and ζ_f correspond to Slater–Condon electrostatic and spin–orbit integrals, respectively; f_k and A_{SO} represent matrix elements for the angular parts of these electrostatic and spin–orbit interactions. The term H_{IN} takes into account several higher-order corrections needed accurately to describe the free-ion energy levels, as explained in detail elsewhere [17]. For our purposes here it is sufficient to note that the adjustable parameters associated with H_{IN} are α, β and γ as well as T^i ($i = 2, 3, 4, 6, 7, 8$), M^h ($h = 0, 2, 4$), and P^f ($f = 2, 4, 6$), as used in f-element spectroscopy. The appropriate values of these and all other free-ion parameters used in our calculations have been approximated by corresponding energy-level parameters for Ln^{3+}: LaF_3 given in table 1 of the survey by Carnall *et al* [17]. Although our data are not extensive enough to permit us to observe highly excited electronic states of the $R123O_7$ systems or to assign values for the large number of free-ion parameters, we do need to take these parameters into account to obtain reliable eigenfunctions and magnetic properties for the lowest electronic states of the f^n configuration.

The part of the Hamiltonian with which we are most concerned is the crystal-field term

$$H_{CF} = \sum_{k,q,i} B_q^k C_q^k(i).$$

$C_q^k(i)$ gives the matrix elements of the qth component of a spherical tensor of rank k for the ith electron. The symmetry of the site occupied by the f-element determines which of the adjustable parameters B_q^k can have non-zero values.

The crystal-field site symmetry of the rare earth in the $Y123O_7$-type orthorhombic structure is *mmm* (D_{2h}) [19]. A crystal field with this symmetry is characterized by nine real parameters: B_0^2, B_0^4, B_0^6, B_2^2, B_2^4, B_4^4, B_2^6, B_4^6, B_6^6. (It is worth noting here that the values of these non-zero crystal-field parameters have a symmetry property also. Simultaneously reversing the signs of B_2^2, B_2^4, B_2^6, and B_6^6 leaves all the crystal-field energy levels and magnetic-dipole transition strengths unchanged. These two phase choices correspond to a rotation by 90° around the z-axis for the x- and y-axes used to define the crystal-field parameters.) A site with this symmetry will, in principle, fully split the Pr^{3+} ground term ($4f^2$, $^3H_4$) into nine energy levels, and the Nd^{3+} ground term ($4f^3$, $4I_{9/2}$) into five Kramers doublets. Since we have either too many observed features (ten or more) for $Pr123O_7$, or too few (only four observed lines from $Nd123O_7$) we cannot initially determine the nine crystal-field parameters for these compounds directly from our measured spectra. Instead, we have started from the level assignments for $Ho123O_7$ based on the detailed measurements of Furrer *et al* [10] to obtain values for the B_q^k

parameters of Ho^{3+}. Then we have re-scaled these values to approximate the parameters expected for Nd^{3+} and Pr^{3+}.

As explained in paper I, we chose Ho^{3+} as our reference because its ground-state term yields the largest number of crystal-field energy levels in the rare earth series and because $Ho123O_7$ has been the subject of a careful, detailed study [10]. Initially, we looked at several different starting points from which to interpret the inelastic neutron data presented by Furrer *et al* [10], but after investigating several approaches, we found that while we could find other sets of assignments and corresponding parameters which reproduced the peak positions, only the assignments reported by the previous authors satisfactorily reproduced both the peak positions and the relative intensities, as these authors had already observed [10]. However, Furrer *et al* use the Stevens operator-equivalents formalism [20], which only considers effects within the ground-term J multiplet of f^n. We, on the other hand, include up to the 100 lowest energy states of the f^n configuration (or, for the f^2 configuration, all 91 states) in our calculation of magnetic properties. To obtain parameter values consistent with our calculations we had to re-fit the nine crystal-field parameters. We used the assignments of ten observed excitation energies made by Furrer *et al* and followed standard procedures [18] to adjust the nine crystal-field parameters. This least-square fit has only one degree of freedom. The parameters represent the data for $Ho123O_7$ quite well and another test for them, as discussed below, comes in the comparison between our data for Nd and $Pr123O_7$ compounds with calculations based on crystal-field parameters that we have extrapolated for these lighter rare earths based on the values for Ho^{3+}.

It is important to note the different conventions for defining crystal-field parameters used in the Stevens operator-equivalent formalism and in the irreducible-tensor formalism. This relationship has been well analysed by Kassman [21]. We adopt his practice of using A_k^q for Stevens parameters and B_q^k for tensor parameters. This practice differs from that of Furrer *et al* but agrees with that used by Carnall *et al* [17]. In order to call attention to our use of tensor crystal-field parameters and to facilitate comparison of our values with other tensor parameters deduced from optical spectroscopy, we give our energy parameters in units of cm^{-1} even though we tabulate the calculated and observed energy levels in units of meV (1 meV = 8.066 cm^{-1}). In table 1 we give the crystal-field parameters of Furrer *et al* [10], translated into the tensor conventions, in the second column. In columns three and four we give our two sets of re-fitted crystal-field parameters for Ho^{3+}. The first re-fitted set of B_q^k values is based directly on the original detailed assignments of Furrer *et al*. The second set of re-fitted B_q^k values is based on a slight readjustment of the detailed positions for the energy levels as suggested by the calculated magnetic transition strengths for each transition. The desirability of this 'fine tuning' in the assignments for $Ho123O_7$ was indicated by our analysis of $Pr123O_7$. It is clear that the changes in the values of the crystal-field parameters produced by our re-fitting procedure has not changed the overall distribution of large versus small values or the signs of the larger parameters. Probably the differences between the parameter set given by Furrer *et al* and our parameter sets for $Ho123O_7$ are well within the experimental uncertainties about the locations of peak positions for the higher excited states.

Table 2 lists the calculated 17 lowest energy levels obtained by using these crystal field parameters together with the free-ion parameters for Ho^{3+} from the tabulation of Carnall *et al* [17]. All these calculations of optical and magnetic properties of $Ho123O_7$ have been carried out using the 92 lowest-energy basis states. In table 2 we also give the calculated magnetic transition strengths parallel and perpendicular to the principal

Table 1. Crystal-field parameters for Ho^{3+}, Nd^{3+}, and Pr^{3+} in the $R123O_7$ crystal environment. All values are given in cm^{-1}.

	Ho^{3+}			Nd^{3+}		Pr^{3+}	
		This work					
Crystal field parameters	Ref. [10] (cm^{-1})	Refit† (cm^{-1})	Best assign‡ (cm^{-1})	Scaled (cm^{-1})	Best fit (cm^{-1})	Scaled (cm^{-1})	Best fit (cm^{-1})
B_0^2	333.7	458.5	434.8	406.4	416.8	440.3	451.60
B_0^4	−1763.2	−2120.0	−1907.5	−2559.3	−2712.4	−3015.9	−2773.13
B_0^6	448.8	500.9	471.6	841.9	620.7	1067.0	786.64
B_2^2	59.27	91.95	76.6	81.51	148.4	88.24	160.81
B_2^4	18.38	−35.59	−297.4	−42.95	11.74	−50.62	13.83
B_4^4	972.7	988.8	1050.1	1193.1	1669.4	1406.1	1491.3
B_2^6	−26.26	−86.30	−252.6	−145.0	−268.6	−183.8	−340.39
B_4^6	1199.6	1311.1	1305.1	2203.6	1978.2	2792.8	2612.54
B_6^6	−12.4	−2.25	−14.78	−3.72	82.6	−4.79	104.72

† This work obtained by refitting the assignments of Furrer *et al* [10] using 92 states.
‡ This work obtained by revising the assignments and then fitting.

optical symmetry axis. These transition strengths are given from each of the three lowest energy states to the other states within the group of 17 states that were accessible for inelastic scattering in the experiments of Furrer *et al*. Table 2 also includes, in the first column, the observed transition energies identified by Furrer *et al*.

When we scale the crystal-field parameters for Ho^{3+} to obtain corresponding values for Pr^{3+} and Nd^{3+}, there are two contributions to the change of parameter values that we must consider.

(i) Variations in the external, electric field that arise from the crystal environment around the f element.

(ii) Effects of the lanthanide contraction on spatial extent of the f-orbital wavefunctions as one advances through the rare earth series.

This change in the f-orbital wavefunction influences how sensitive f-electron energy levels are to their environment. There are only small changes in the lattice constants in passing from $Ho123O_7$ to $Pr123O_7$ [4, 22]. Moreover, our molecular-orbital calculations for $R123O_7$ with R = Y, Pr, Nd, Ho and Cm indicate very little change in charge distributions for the rare earth compounds studied [6]. Therefore, we have assumed initially that the external electric field is effectively constant for the cases of interest here. We focus our attention on estimating the effect of changes in the radial extent of the f-orbitals.

Since we are trying only to account for gross trends in the behaviour of f-wavefunctions within the lanthanides, it seems sufficient, and is most convenient, to look at classic Hartree–Fock results. In their table VII Freeman and Watson give calculated values of the radial averages $\langle r^k \rangle$, $k = 2, 4, 6$ for selected lanthanide 3+ ions [23]. This tabulation includes values for Pr^{3+} and Nd^{3+} but not Ho^{3+}. We have interpolated an average of values listed for Dy^{3+} and Er^{3+} as our estimate for the corresponding values for Ho^{3+}. On this basis we expect the second-rank crystal field parameters, i.e.

B_0^2 and B_2^2, for Pr^{3+} and for Nd^{3+} to be 1.56 and 1.44, respectively, times the corresponding parameters for Ho^{3+}. For fourth-rank parameters these ratios are 2.31 and 1.96; and for sixth-rank parameters they are 3.46 and 2.73. When we used crystal-field parameters for $Nd123O_7$ obtained by multiplying the corresponding Ho values by the appropriate ratios, the calculated energy levels agreed with the general pattern of transition energies observed for $Nd123O_7$. But the calculated energy levels spread over a larger energy range than did the observations. Clearly the Hartree–Fock calculations overestimate the influence of the lanthanide contraction on the crystal-field parameters. This overestimation is sometimes corrected by using shielding constants, σ_k, that are different for each tensor rank k [24]. We decided for simplicity to multiply all of our extrapolated crystal-field parameters by one adjustable re-scaling factor to make the overall width of calculated spectrum for $Nd123O_7$ agree with the experimental width. The value of 0.6156 for this re-scaling factor gives good agreement between the observed and calculated energy levels†.

Our scaled crystal-field parameters for Nd^{3+} based on scaling ratios relative to Ho^{3+} of 0.886, 1.207 and 1.681 for $k = 2$, 4 and 6, respectively, are given in the fifth column of table 1. In table 3 the corresponding calculated energy levels (column 4) are compared to the observed transition energies (columns 1–3). The agreement with the observed transition energies seems good except for the difference in position of the first excited energy level (observed at 12 meV and calculated near 4 meV). This scaled calculation yields a ground state magnetic moment along the crystallographic c axis of 1.71 μ_B that disagrees with the saturation moment of 1.1 μ_B observed for the antiferromagnetic ordered state of $Nd123O_7$ [28, 29]. Therefore, we have tried to improve our crystal-field parameters for Nd^{3+} by varying the parameters B_0^4, B_4^4 and B_4^6 to fit the observed inelastic scattering peak positions. Column 6 in table 1 gives our 'best fit' crystal-field parameters for $Nd123O_7$. Crystal-field parameters that were not varied in this case have been obtained by scaling the corresponding best-fit parameters that we obtain below by fitting the observed spectrum of $Pr123O_7$. In table 3 column 5 gives the 'best fit' calculated energy levels for $Nd123O_7$ and columns 6–9 give the corresponding transition strengths connecting the two lowest levels with excited levels arising within the $^4I_{9/2}$ ground-state

† The question naturally arises: how reasonable is the purely empirical value of 0.6156 for the re-scaling factor that we have introduced for Nd^{3+}? This re-scaling factor corrects the Hartree–Fock scaling ratios for 3+ ions to produce calculated crystal-field levels in closer agreement with those observed experimentally. This re-scaling corresponds to reducing the influence of the lanthanide contraction to account for effective charges less than 3+ on the lanthanide ions, such as those indicated by our molecular orbital calculations for R123O7 crystals [6, 25]. This type of adjustment of the Hartree–Fock ratios for the $\langle r^k \rangle$ radial averages of 3+ ions is not usually made in studies of the influence of crystal-field splitting on magnetic susceptibilities that adequately explain the observed relationships between properties of analogous compounds of different lanthanide elements. See for example, [26] and [27]. However, in studies of primarily magnetic properties, any values for crystal-field parameters are observed much less directly than they are in optical absorption studies, such as those analysed by Carnall *et al* [17] for Ln^{3+} in LaF_3. Using the ratios of parameters for Pr^{3+} and Nd^{3+} to those for Ho^{3+} as given by Carnall *et al*, we conclude that our re-scaling of the Freeman–Watson Hartree–Fock values seems very reasonable. In this comparison we have averaged over all permitted values of q, for each value of k, using the ratios $B_q^k(\mathrm{Ln})/B_q^k(\mathrm{Ho})$, of the values given in table 1 of [17] for Ln = Pr and Nd. In this way for Pr to Ho, we find ratios of 1.014, 1.455, and 1.595 for $k = 2, 4$, and 6, respectively; correspondingly, for Nd to Ho, we find 0.758, 1.393 and 1.620. In order to simplify the comparison with calculated values, we average these numbers for Pr and Nd to obtain empirical values of 0.886, 1.424, and 1.607, for scaling ratios of second, fourth and sixth rank tensor parameters between the lighter and heavier lanthanide compounds. The corresponding calculated values are 1.500, 2.135, and 3.095 for the Freeman–Watson results for 3+ ions; and 0.923, 1.314, and 1.905, after re-scaling by 0.6156. The agreement between empirical and calculated ratios is clearly better after re-scaling.

Table 2. Observed and calculated energy levels for $Ho123O_7$ and calculated magnetic transition strengths within the ground term, $^5I_8$, for Ho^{3+}. The calculated energy levels are all non-degenerate with the indicated symmetry classification for our assigned best fit given in column 4. The calculated transition strengths are given originating from the three lowest energy levels: *A*, the ground level; *B*, the first excited level; and *C*, the second excited level.

Observed energy [10] (meV)	Calculated [10] (meV)	Energies This work Refit† (meV)	Best assign‡ (meV)	Γ_n n	Magnetic transition strengths (μ_B^2) $\|\mu_\parallel\|^2$	$\|\mu_\perp\|^2$	$\|\mu_\parallel\|^2$	$\|\mu_\perp\|^2$	$\|\mu_\parallel\|^2$	$\|\mu_\perp\|^2$
					A		*B*		*C*	
0	0	0	0	3	0	0	0	10.61	0	14.17
0.5	0.13	0.20	0.73	2	0	10.61	0	0	29.20	0
1.8	1.28	1.62	2.03	4	0	14.17	29.20	0	0	0
3.8	3.60	4.06	3.79	1	14.02	0	0	6.26	0	1.60
4.3	3.81	4.16	4.23	3	0	0	0	15.17	0	5.47
8.1	7.61	8.14	8.37	1	21.74	0	0	0.42	0	8.86
10.8	10.28	10.56	11.36	2	0	3.42	0	0	6.86	0
11.6	10.75	11.52	12.05	4	0	5.84	4.07	0	0	0
—	50.99	54.87	53.86	3	0	0	0	0.31	0	2.79
—	51.44	57.62	56.61	1	0.37	0	0	0.09	0	0.59
59	53.42	58.61	58.76	4	0	1.14	2.22	0	0	0
59	53.54	58.90	59.26	2	0	0.86	0	0	2.89	0
—	53.71	59.02	61.51	3	0	0	0	0.64	0	0
—	57.00	63.73	62.76	1	0.25	0	0	1.62	0	0.09
70	62.81	69.31	69.01	2	0	0.51	0	0	3.11	0
—	63.35	69.98	69.82	4	0	0.25	2.84	0	0	0
73	65.88	72.91	73.16	1	1.57	0	0	1.51	0	1.17

† This work obtained by refitting the assignments of Furrer *et al* [10] using the 92 lowest-energy crystal-field states of f^{10}.

‡ This work obtained by revising the assignments and refitting using the lowest 92 states.

term of Nd^{3+}. Now the agreement with the inelastic scattering data is excellent for both positions and relative intensities of the observed transition. Figure 1 of our experimental paper [1] illustrates the comparison. Moreover, the calculated value of 1.11 μ_B for $\mu_\parallel$ also agrees with observations of the antiferromagnetic ordered moment [28, 29].

Crystal-field parameters for $Pr123O_7$ were predicted by combining scaling ratios from the Hartree–Fock results with the re-scaling factor determined by comparison with the experimental spectrum for $Nd123O_7$. The resulting scaling ratios for the B_q^k values of Pr^{3+} relative to those of Ho^{3+} are 0.960, 1.422 and 2.130, for $k = 2$, 4 and 6, respectively. The extrapolated crystal-field parameters, as given in the seventh column of table 1, were then used to predict the expected energy levels for $Pr123O_7$. The predicted line positions are listed in the second column of table 4. In the first column of table 4, we give the observed peak centres that are assigned to correspond with our calculated levels. In general, with the exception of the first excited level, the agreement between observed and calculated energies is satisfactory. But the comparison between the observed peak sizes and the calculated transition strengths associated with these initial predictions is less satisfactory. For example, the intensity calculated for the level at 110 meV in this first prediction is greater than that for the levels near 80 and those near 65 meV.

Table 3. Observed and calculated energy levels for $Nd123O_7$ and calculated magnetic transition strengths within the ground term, $^4I_{9/2}$, for Nd^{3+}. The calculated energy levels are all doublets with no distinctions in symmetry classification. The calculated transition strengths are given originating from the two lowest levels: *A*, the ground level and *B*, the first excited level.

Obs energies			Calc energy		Magnetic transition strengths (μ_B^2)			
[11] (meV)	[12] (meV)	This work† (meV)	Scaled (meV)	Best fit (meV)	$\lvert\mu_\parallel\rvert^2$	$\lvert\mu_\perp\rvert^2$	$\lvert\mu_\parallel\rvert^2$	$\lvert\mu_\perp\rvert^2$
					A		*B*	
0	0	0	0	0	1.23	1.68	0.039	0.003
	5.84‡							
12	12.6	12	3.85	12.18	0.039	0.003	1.16	1.88
20	21.5	20.8	25.23	20.41	2.72	0.27	0.45	1.08
36		36	38.36	36.16	0.19	1.12	1.08	0.69
		117	117.4	116.98	0.73	0.19	0.022	0.88

† See our experimental paper I [1].
‡ See text for assignment to Nd ions on Ba sites.

Table 4. Observed and calculated energy levels for $Pr123O_7$ and calculated magnetic transition strengths within the ground term, $^3H_4$, for Pr^{3+}. The calculated energy levels are all non-degenerate with the indicated symmetry classification Γ_n. The calculated transition strengths are given originating from the three lowest energy levels: *A*, the ground level; *B*, the first excited level; and *C*, second excited level.

Obs energy (meV) See text	Calc energies		Symmetry Γ_n n	Magnetic transition strengths (μ_B^2)					
	Scaled (meV)	Fitted (meV)		$\lvert\mu_\parallel\rvert^2$	$\lvert\mu_\perp\rvert^2$	$\lvert\mu_\parallel\rvert^2$	$\lvert\mu_\perp\rvert^2$	$\lvert\mu_\parallel\rvert^2$	$\lvert\mu_\perp\rvert^2$
				A		*B*		*C*	
0	0	0	1	0	0	0	1.65	0	2.10
1.4	0.175	1.4	4	0	1.65	0	0	4.40	0
3.9	3.68	3.8	2	0	2.10	4.40	0	0	0
35†									
45	44.37	44.8	1	0	0	0	0.13	0	0.12
50	53.22	49.8	3	0.12	0	0	0.64	0	0.30
65	66.83	64.8	2	0	0.54	0.64	0	0	0
80	76.40	79.6	4	0	0.40	0	0	0.52	0
85‡	85.32	84.5	3	1.85	0	0	0.20	0	0.42
105‡	110.00	104.5	1	0	0	0	0.67	0	0.54
113†‡									
123†‡									

† See text for assignment.
‡ Taken from [13].

We found that a relatively small adjustment of the assignments in terms of the symmetry of the crystal-field states associated with particular observed energy levels permits us to do a good fit of the B_q^k parameters for Pr^{3+} in $Pr123O_7$. These fitted

We have followed the conventions for symmetry classifications for D_{2h}-states that are described by Furrer *et al* [10]. Calculated transition strengths are listed from the three lowest energy levels to the other levels arising within the ground term for f^2, $^3H_4$. By taking into account thermal occupation at 25 K for the excited levels, we now find good agreement with the intensities as well as the positions of the assigned spectral features, as illustrated in figure 1(b). Some of these assigned features such as those near 45 and 50 meV are very weak and have transition strengths from the lowest crystal-field level that are, respectively, 0 and 1/50 times the strength to the excited level at 85 meV. We are not assigning the spectral feature near 35 meV to an electronic level of $PrBa_2Cu_3O_7$ as explained above.

In the next section we use the crystal-field states of the f^2 configuration of Pr^{3+} corresponding to our assignments of inelastic neutron scattering features to calculate magnetic and thermodynamic properties of $PrBa_2Cu_3O_7$.

3. Magnetic and thermodynamic properties of $PrBa_2Cu_3O_7$

Using eigenvectors of f^2 crystal-field states in the van Vleck formalism [1, 30], we have calculated magnetic susceptibilities of Pr^{3+} in $PrBa_2Cu_3O_7$ both parallel and perpendicular to the crystal-field z-axis, $\chi_\parallel$ and $\chi_\perp$, respectively; as well as, calculated $\chi_{ave} = (\chi_\parallel + 2\chi_\perp)/3$. Recent work on the relation of crystal-field parameters for tetragonal and for orthorhombic $HoBa_2Cu_3O_7$ [31] leads us to conclude that the z-axis to which our crystal-field calculations refer is the c-axis of the crystal. Thus, we identify $\chi_\parallel$ with χ_c. Moreover, the corresponding calculated parallel magnetic moments $\mu_\parallel$ can be compared with the observed low-temperature ordered moment along this c-axis in the antiferromagnetically ordered phase of $PrBa_2Cu_3O_7$ studied by Li *et al* using neutron diffraction [8].

The anisotropy of the calculated susceptibility depends strongly on the choice of ground state for Pr^{3+}. But the average susceptibility χ_{ave} is rather insensitive to these changes. Magnetic susceptibility observations for powder samples are compared to the calculated values of χ_{ave} in I [1].

The predicted values of $\chi_\parallel$ and $\chi_\perp$ for the fitted crystal-field parameters of $PrBa_2Cu_3O_7$ are roughly equal around 100 K, with $\chi_\parallel$ being smaller than $\chi_\perp$ for lower temperatures and a little larger, for higher temperatures. The predicted magnetic anisotropy is much greater for our initial estimate for crystal-field parameters of $PrBa_2Cu_3O_7$. This estimate was obtained by scaling tensor crystal-field values for $HoBa_2Cu_3O_7$ and is reported in the seventh column of table 1. These scaled crystal-field parameters lead to $\chi_\parallel$ about twice $\chi_\perp$ near 40 K and about 5/4 times as large near 300 K. Figure 3(a) gives plots of the average susceptibilities for comparison to experimental values obtained with powder samples. Figure 3(b) shows plots of the corresponding predicted magnetic anisotropies. We think that experimental investigation of the magnetic anisotropy for $PrBa_2Cu_3O_7$ would be useful to confirm symmetry assignments for the observed crystal-field energy levels.

Our crystal-field calculation reported in the previous section of this paper and summarized in paper I completely ignores the type of interactions between f-electrons on different Pr atoms that produce magnetic ordering. When these cooperative interactions are ignored we find, as previously mentioned, that the crystal-field predicts very small splittings of the three lowest lying states: $\varphi_\pm$ and φ_0, say. These crystal-field states have

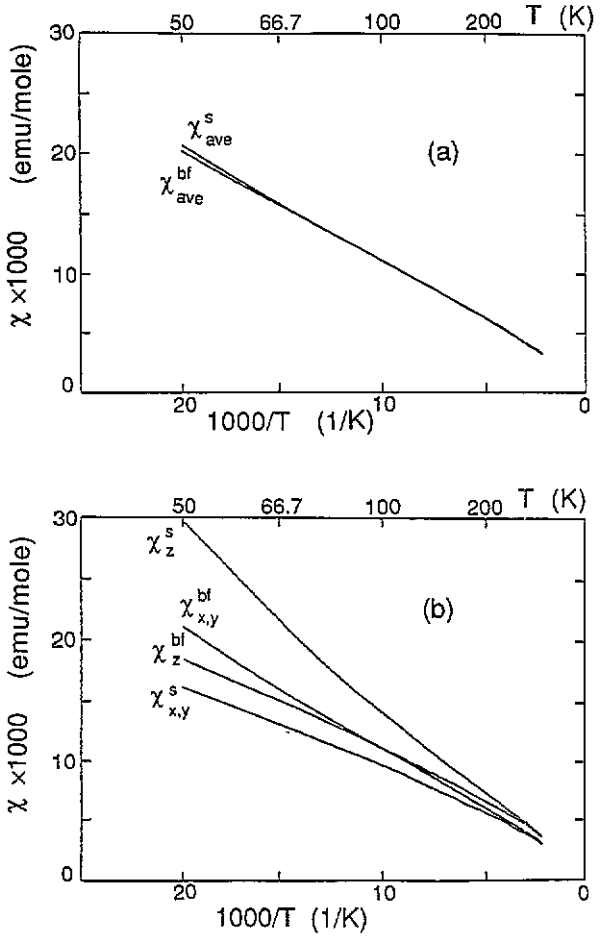

Figure 3. Calculated magnetic susceptibilities for $PrBa_2Cu_3O_7$ as functions of the inverse temperature. They are shown for both the original scaled parameter set (χ^s) and the best-fit parameter set (χ^{bf}). Plots are given for three susceptibilities in each case $\chi_{ave} = (\chi_z + \chi_x + \chi_y)/3$, $\chi_\parallel = \chi_z$, and $\chi_\perp = \chi_{x,y} = (\chi_z + \chi_y)/2$.

eigenfunctions that can be reasonably represented (i.e. with 90% reliability) in terms of components of the $^3H_4$ states as follows:

$$\varphi_\pm = \frac{1}{\sqrt{2}}(|J = 4, M = +3\rangle \pm |J = 4, M = -3\rangle)$$

and

$$\varphi_0 = \frac{1}{\sqrt{2}}(|J = 4, M = +2\rangle + |J = 4, M = -2\rangle).$$

How well do these $\varphi_\pm$, φ_0 states represent magnetic properties of the lowest-energy states in our crystal-field calculation? First of all, all diagonal matrix elements of the magnetic moment vanish for these $\varphi_\pm$, φ_0 states (as they must for any non-degenerate crystal-field eigenstate). Since the g factor for $^3H_4$ states is 0.8, we have $0.8 \times 3 = 2.40\ \mu_B$

for $\mu_\parallel$ connecting these two $\varphi_\pm$ states in this model. This value is to be compared with $2.10\,\mu_B$ that comes from our 91 state calculation of magnetic properties. Perpendicular components of the magnetic transition moments connecting the two $\varphi_\pm$ states vanish by symmetry. Between φ_0 and $\varphi_\pm$ the parallel transition moments vanish by symmetry and the perpendicular components are $0.8 \times \sqrt{3.5} = 1.50\,\mu_B$, to be compared with 1.45 and $1.28\,\mu_B$ from our 91 state calculation of magnetic properties.

The states of the individual neighbouring Pr^{3+} ions, represented by $\varphi_\pm$ and φ_0, can be coupled in the crystal lattice by a cooperative interaction between neighbouring Pr ions. Competing influences of the isolated-ion crystal field and the interaction between ions determine the actual renormalized wavefunctions and resulting saturation moment for the antiferromagnetic ordered phase. Within the framework of our model, interactions between the ions are proportional to the square of the transition moment connecting the crystal-field eigenstates. We consider only the ordering associated with the $\mu_\parallel$ transition moment between the $\varphi_\pm$ states, since it can be expected to produce an interaction between ions more than twice that for the $\mu_\perp$ that connects the φ_0 and $\varphi_\pm$ states and also because the measured ordered moment for $Pr123O_7$ lies along the crystal c axis that corresponds to our $\mu_\parallel$ [8].

Our approach to analysing the cooperative phenomena is based on what has been called the two singlet-level model (see references [16] and [32]). The model for the mixing of the low-lying crystal-field $\varphi_\pm$ states is made more specific in terms of the crystal-field splitting energy Δ_{CF} between these $\varphi_\pm$ states and the interaction energy of a particular Pr ion with its nearest neighboring Pr ions E_I. The effective single-site energy matrix then takes the following form in this $\varphi_\pm$ basis:

$$\begin{bmatrix} +\Delta_{CF}/2 & E_I \\ E_I & -\Delta_{CF}/2 \end{bmatrix}.$$

Let us think of the single-site Pr-ion ground state in the magnetically ordered crystal as having two eigenvalues E_- and E_+, with their respective eigenfunctions $\Psi_-(\theta)$ and $\Psi_+(\theta)$ that are mixtures of the two $\varphi_\pm$ crystal-field states:

$$\Psi_-(\theta) = \varphi_- \cos\theta - \varphi_+ \sin\theta$$

and

$$\Psi_+(\theta) = \varphi_+ \cos\theta + \varphi_- \sin\theta$$

where

$$\theta = \tfrac{1}{2}\arctan(2E_I/\Delta_{CF}).$$

Then

$$E_\pm = \pm\tfrac{1}{2}(\Delta_{CF}^2 + 4E_I^2)^{1/2}.$$

In this model, the ground-state ordered moment is given by

$$\mu_{GS} = \langle\Psi_-(\theta)|\mu_z|\Psi_-(\theta)\rangle = -\tfrac{1}{2}(\langle\varphi_-|\mu_z|\varphi_+\rangle + \langle\varphi_+|\mu_z|\varphi_-\rangle)\sin 2\theta.$$

So that $\mu_{GS} = -\mu_\parallel \sin 2\theta$, in terms of the transition moment $\mu_\parallel$ that has a value of $2.10\,\mu_B$ in our 91-state crystal-field calculation. The observed low-temperature ordered moment is $[\mu_z] = (0.74 \pm 0.08)\,\mu_B$ [8]. Equating the magnitudes of $[\mu_z]$ and μ_{GS}, we find a corresponding mixing angle of $\theta = \pm 10.3°$. In the previous sections, we showed that Δ_{CF} between the states φ_- and φ_+ is $3.9 - 1.4 = 2.5$ meV or 29 K. Combining these values

for θ and Δ_{CF}, we find $E_I = \pm 5.5$ K (some 0.47 meV) for the effective interaction between neighbouring Pr^{3+} ions. We note that this value for the Pr–Pr interaction energy is a factor of eight smaller than the Lorentzian full width at half maximum (FWHM) 3.8 meV that we found above for the neutron inelastic scattering features of $Pr123O_7$ in figure 2.

If the Pr–Pr interaction energy is substantially smaller than the intrinsic width of the neutron scattering features, other non-Pr contributions must be considered. It is tempting to speculate that they arise from the conduction electrons as well as the Cu and the O atoms. This point of view is consistent with the requirement for a mechanism that produces 3D ordering along the *c* axis for distant Pr moments to involve interactions with the intervening Cu, O and other electrons in the crystal.

This interpretation of the low-temperature ordered moment still leaves unanswered questions about the relationship of the effective interaction energy to the observed Néel temperature and other thermodynamic properties of $Pr123O_7$. Low-temperature specific heat measurements have recently been reported for dilute samples of $(Y_{1-x}Pr_x)Ba_2Cu_3O_7$ for $x = 0.3$ [33]. Based on Debye temperatures of 330 K for $Pr123O_7$ and 350 K for $Y123O_7$, we have predicted thermodynamic functions for the paramagnetic phase of these materials [34]. Our preliminary comparisons show satisfactory agreement of the observed and calculated values for corresponding specific heat functions at temperatures just above the magnetic ordering temperature. We are encouraged by these initial tests of the correctness of electronic thermodynamic functions calculated from the energy-level assignments given here for $Pr123O_7$.

Calculated thermodynamic functions based on our assignments are consistent also with recently published specific heat observations up to 20 K [8, 15] as well as with other measurements on the paramagnetic phase up to 30 K [35]. By way of contrast, however, our predicted thermodynamic functions for pure $Pr123O_7$ disagree with the first reported specific heat and estimate of the entropy change associated with the magnetic ordering transition in the vicinity of 17 K published in 1988 [9]. These comparisons are shown in figure 4.

In figure 4 we reproduce observed specific heat curves from the literature [8, 15, 9 and 35] in parts (a), (b), (c) and (d), respectively. In each part of figure 4 we have overlaid our predicted specific heat curves. Three calculated curves are shown. These are the total specific heat as a function of temperature, *T*; the lattice contribution; and the contribution from the three lowest-lying energy levels of the f^2-configuration. We have used the Debye heat capacity function $C_V/3R$ [36] to estimate the lattice contribution with a Debye temperature Θ_D of 330 K. We have used three non-degenerate electronic energy levels at 0, 21.4 and 49.9 K to model the Pr^{3+} ion. Because of the flexibility inherent in our choice of Θ_D, slight differences between these thermodynamic levels and the assigned energy levels given in column 1 of table 4 are not significant for the comparisons we are making here.

We can only expect agreement between our calculations and observations in the paramagnetic phase. Figure 4(d) is very useful in making this comparison since the observations extend up to 30 K. Comparison of observations for *T* less than 20 K seems to indicate that in this lower temperature range the sample for 4(d) may not have reached equilibrium following each change in temperature. The specific heat anomaly associated with antiferromagnetic ordering at about 17 K seems rather too small in 4(d) as compared to the other observations.

It is worth noting here that an important test of any model for the electronic structure of $Pr123O_7$ is how well it corresponds to the observed third-law entropy for the material.

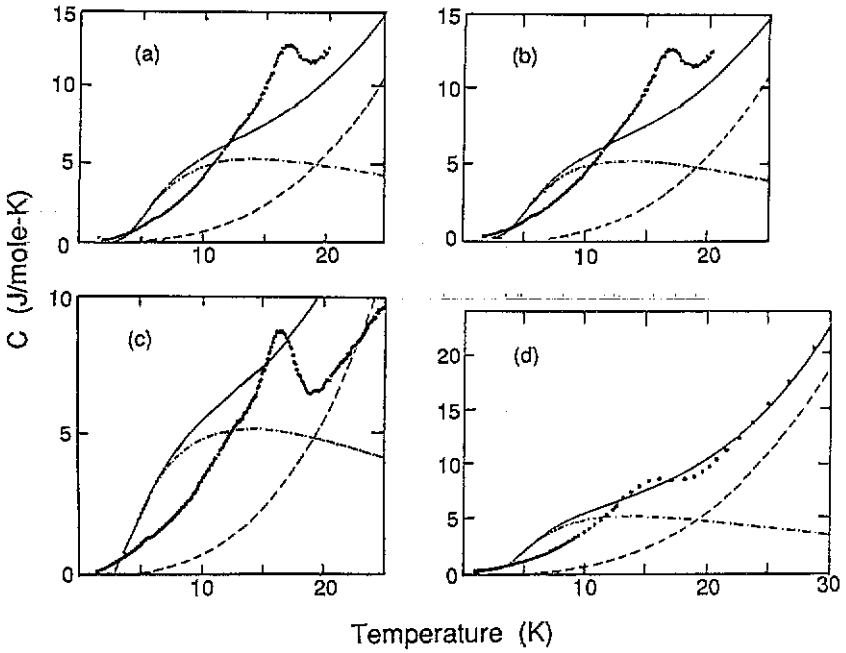

Figure 4. Observed and calculated specific heat curves for $PrBa_2Cu_3O_7$. Observed specific heats are reproduced from the following sources: (a) figure 3(a) of [8], (b) figure 4(a) of [15], (c) figure 1(a) of [9] and (d) figure 10(a) of [35]. In all cases we use a Debye temperature of 330 K. Separate curves show the Debye-function heat capacity for the lattice (broken) and electronic heat capacity of the three level system (chain curve) (see text).

Our model for the crystal-field levels of Pr^{3+} ions in the paramagnetic phase should be compared to the measured third-law entropy after the measured specific heat begins to agree with the calculated specific heat, i.e. at about 30 K and above. Unfortunately the recent, careful low-temperature studies of specific heat only went up to 20 K [8, 15]. Nevertheless, a rough preliminary understanding of the entropy comparison for the paramagnetic phase can be obtained by studying figures 4(a) and (b).

The third-law entropy at a given temperature T corresponding to specific heat measurements from effectively 0 K up to T is given by the $1/T$ weighted area up to that temperature under the curve of the specific heat as a function of T. [37]. Thus, we can look at figures 4(a) and (b) to determine how much difference there will be in the $1/T$ weighted areas under the measured and the predicted specific heat curves. There are two regions of difference in the curves. For an area centred around about 8 K the predicted specific heat is greater than the measured specific heat. For an area centred around 17 K the measured specific heat is greater. The $1/T$ weighting makes the area at the higher temperature approximately half as effective for increasing the entropy as that at the lower temperature at which the two specific heat curves differ. Although it is somewhat subjective until careful specific heat measurements are published up to 30 K, it looks as though the area of difference between the two specific heat curves around 8 K is about half of the area of difference around 17 K, provided that the two curves do come together at a temperature between 25 and 30 K. If this estimate is correct, by 30 K or so, the measured and predicted third-law entropies would agree. As shown in figure 4(d) the measured and the predicted specific heat curves do seem to have equal values, slopes

and curvatures between 25 and 30 K so that the curves and their integrals should continue to agree above 30 K. It will be interesting to see how these thermodynamic comparisons hold up for more complete data.

4. Discussion and summary

We have explained the details of the scaling procedure that provides the framework within which we have assigned the observed inelastic neutron scattering peaks of $Nd123O_7$ and $Pr123O_7$. These assignments are completely consistent with corresponding assignments by Furrer *et al* for similar data of the analogous Ho compound [10]. We think that analysis of crystal-field levels for other rare-earth ions substituted into the $R123O_7$ lattice will also be aided by predictive energy-level calculations based on appropriately scaled B_q^k parameters. Now that fitted values for these parameters are available for both light, Pr and Nd, and heavy, Ho, members of the lanthanides, we hope that a simple linear scaling proportional to the change in the number of f-electrons may be adequate for initial estimates. The involved procedure that we used, relying on Hartree–Fock results to extrapolate the values for Ho to the lighter lanthanides, may not be needed again for this class of compounds.

Based on the available neutron scattering data for the paramagnetic phase of $Pr123O_7$, we have given 'consensus' values for the crystal-field parameters in this phase and deduced an intrinsic Lorentizian width of 3.8 meV for the neutron inelastic scattering features of $Pr123O_7$. The resulting crystal-field eigenfunctions and eigenvalues have been used in standard crystal-field theory to predict the anisotropic magnetic susceptibility and other properties for Pr^{3+} in $Pr123O_7$. Previously we showed that the calculated magnetic susceptibilities for powder samples agree very well with those found experimentally [1]. Our simple crystal-field model for Pr^{3+} ions predicts the unexpectedly low effective paramagnetic moment found experimentally for $Pr123O_7$.

In this paper we have predicted the anisotropies of the magnetic susceptibility for $Pr123O_7$ and showed how these anisotropies can help to distinguish between competing models for describing the lowest three energy levels of the f^2 configuration in this crystal. These three electronic states would all be degenerate in the cubic crystal-field that forms the dominant component of the observed local electric field. The details of how this threefold degeneracy is lifted in the $R123O_7$ lattice are most physically important. Thus, there is good reason to hope that experimental studies of magnetic susceptibilities of single-crystals, or at least oriented samples, of $Pr123O_7$ will substantially advance confidence in the details of the non-cubic parts of the crystal-field environment of the Pr^{3+} ions in this lattice.

Also in our present paper, we discuss a primitive two-singlet-states model for interactions between neighbouring Pr^{3+} ions. This model allows us to understand the relatively small low-temperature ordered moment observed for the antiferromagnetic phase. Thus, we provide additional support for our conclusion that standard crystal-field theory correctly applied to the f^2 configuration for Pr^{3+} ions fully explains the unusual magnetic properties of $Pr123O_7$. The fundamental feature of the antiferromagnetically ordered phase is that each Pr ion site experiences a strong local magnetic field parallel to the *c*-axis of the crystal. This strong local magnetic field causes renormalization of the crystal-field states. States that are linked by sizeable off-diagonal matrix elements of $\mu_\parallel$, the magnetic moment parallel to the *c* axis, are mixed with each other to form these renormalized states. The competition between the original crystal-field splittings and the induced magnetic moment splittings results in some specific

amount of mixing in the ordered state. We found that a mixing of only 3%, corresponding to a mixing angle of $\pm 10.3°$, was sufficient to account for the observed ordered moment of 0.74 μ_B found in the antiferromagnetic phase [8].

Taking the argument a little farther we reason that the very strong local magnetic field at each Pr site in the lattice strongly influences all five crystal-field states that are connected to each other by large off-diagonal magnetic moments (1.8, 2.1, 2.5 μ_B) parallel to the *c* axis. Because the excited states at 1.4 and 3.8 meV are linked by an off-diagonal $\mu_\parallel$ of 2.1 μ_B, these two states are renormalized, as explained in section 3, to produce the observed ordered moment in the antiferromagnetic phase. The three excited states at energies of 44.8, 49.8 and 104.5 meV in the paramagnetic phase are linked by off-diagonal values of $\mu_\parallel$ of 2.5 and 1.8 μ_B, respectively. Thus we expect these states to be mixed with each other and shifted in energy in the antiferromagnetically ordered phase.

Two clear features at higher scattering energies in the 2 K spectra reported by Paul *et al* [13], particularly, 113 and 123 meV, are not consistent with energy levels of the paramagnetic phase as analysed here. These features do not fit into our assigned crystal-field levels for isolated Pr^{3+} ions in the paramagnetic phase nor do they show up in the 25 K spectra for the paramagnetic phase as reported in figure 1(b). It will be very important to learn whether these features depend on the transition to a low-temperature ordered phase of $PrBa_2Cu_3O_7$.

We have given several predictions for thermodynamic functions based on our view of the electronic structure for the paramagnetic phase of $PrBa_2Cu_3O_7$ that should be tested experimentally. Initial comparisons with published data are encouraging and indicate the need for additional measurements of the specific heat in the range 20–35 or 40 K. Tests of our predictions for the third-law entropy in the neighbourhood of 30 K will be very important in confirming or providing data to modify our model for the electronic properties of individual Pr^{3+} ions in the paramagnetic phase.

We are striving for a sound understanding of the electronic properties of isolated Pr ions in the paramagnetic $PrBa_2Cu_3O_7$. Investigators studying cooperative phenomena like magnetic ordering and superconductivity can then build with confidence on such a foundation. In our studies, we have found a value of 3.8 meV for the intrinsic Lorentzian FWHM associated with neutron scattering features of paramagnetic $PrBa_2Cu_3O_7$. This intrinsic width is about eight times larger than the Pr–Pr interaction that can account for the ordered moment in antiferromagnetic $PrBa_2Cu_3O_7$. We hope that these observations may help lead to a physically correct model for understanding cooperative phenomena in this interesting substance.

Acknowledgments

We thank Dr B D Dunlap and Dr H B Radousky for helpful discussions. This work is supported by the US DOE, Basic Energy Sciences–Chemical and Materials Science, and has benefitted from the use of the Intense Pulsed Neutron Source at Argonne National Laboratory, all under contract W-31-109-ENG-38.

References

[1] Soderholm L, Loong C-K, Goodman G L and Dabrowski B D 1990 *Phys. Rev.* B at press
[2] Pickett W E 1989 *Rev. Mod. Phys.* **61** 433
[3] Soderholm L, Zhang K, Hinks D G, Beno M A, Jorgensen J D, Segre C U and Schuller I K 1987 *Nature* **328** 604

[4] Soderholm L and Goodman G L 1989 *J. Solid State Chem.* **81** 121
[5] Soderholm L, Goodman G L, Welp U, Williams C W and Bolender J 1989 *Physica* C **161** 252
[6] Goodman G L and Soderholm L 1990 Physica C **171** 528
[7] Narlikar A V, Narasimha Rao C V and Agarwal S K 1989 *Studies of High Temperature Superconductors* vol 1, ed A Narlikar (New York: Nova Science) ch 15, p 341, and references therein
[8] Li W-H, Lynn J W, Skanthakumar S, Clinton T W, Kebede A, Jee C.-S, Crow J E and Mihalisin T 1989 *Phys. Rev.* B **40** 5300
[9] Jee C.-S, Kebede A, Yuen T, Bloom S H, Kuric M V, Crow J E, Guertin R P, Mihalisin T, Myer G H and Schlottmann P 1988 *J. Magn. Mater.* **76, 77** 617
[10] Furrer A, Bruesch P and Unternahrer P 1988 *Phys. Rev.* B **38** 4616
[11] Allenspach P, Furrer A, Bruesch P and Unternahrer P 1989 *Physica* B **156, 157** 864
[12] Walter U, Holland-Moritz E, Serving A, Erle A, Schmidt H and Zirngiebl E 1988 *Physica* C **153–155** 170
[13] Paul D McK, Rainford B D and Osborn R 1989 *ISIS Annual Report* RAL-89-050 Rutherford Appleton Laboratory, UK A128
[14] Gering E, Renker B, Gompf F, Ewert D, Schmidt H, Ahrens R, Bonnet M and Dianoux A 1988 *Physica* C **153–155** 184
[15] Kebede A, Jee C S, Schwegier J, Crow J E, Mihalisin T, Myer G H, Salomon R E, Schlottmann P, Kuric M V, Bloom S H and Guertin RP 1989 *Phys. Rev.* B **40** 4453
[16] Fulde P 1979 *Handbook on the Physics and Chemistry of Rare Earths* ed K A Gschneidner Jr and L Eyring (New York: North-Holland) ch 17, pp 295–386
[17] Carnall W T, Goodman G L, Rajnak K and Rana R S 1989 *J. Chem. Phys.* **90** 3443
[18] Crosswhite H M and Crosswhite H 1984 *J. Opt. Soc. Am.* B **1** 246
[19] Beno M A, Soderholm L, Capone D W II, Hinks D G, Jorgensen J D, Schuller I K, Segre C U, Zhang K and Grace J D 1987 *Appl. Phys. Lett.* **51** 57
[20] Stevens K W H 1952 *Proc. Phys. Soc.* A **65** 209
[21] Kassman A J 1970 *J. Chem. Phys.* **53** 4118
[22] Dunlap B D, Slaski M, Hinks D G, Soderholm L, Beno M, Zhang K, Segre C, Crabtree G W, Kwok W K, Malik S K, Schulter I K, Jorgensen J D and Sungaila Z 1987 *J. Magn. Magn. Mater.* **68** L139
[23] Freeman A J and Watson R E 1962 *Phys. Rev.* **127** 2058
[24] Erdos P and Kang J H 1972 *Phys. Rev.* B **6** 3393, and references therein
[25] Goodman G L, Ellis D E, Alp E E and Soderholm L 1989 *J. Chem. Phys.* **91** 2983
[26] Dunlap B D and Shenoy G K 1975 *Phys. Rev.* B **12** 2716
[27] Dunlap B D, Hall L N, Behroozi F, Crabtree G W and Niarchos D G 1984 *Phys. Rev.* B **29** 6244
[28] Fischer P, Schmid B, Bruesch P, Stucki F and Unternahrer P 1974 *Z. Phys.* B **74** 183
[29] Yang K N, Ferreira J M, Lee B W, Maple M B, Li W.-H, Lynn J W and Erwin R W 1989 *Phys. Rev.* B **40** 10963
[30] van Vleck J H 1932 *The Theory of Electric and Magnetic Susceptibilities* (London: Oxford University Press)
[31] Allenspach P, Furrer A, Bruesch P, Marsolais R and Unternahrer P 1989 *Physica* C **157** 58
[32] Cooper B R 1972 *Magnetic Properties of Rare Earth Metals* ed R J Elliot (New York: Plenum) ch 2, pp 17–80
[33] Amato A, Caspary R, Fisher R A, Phillips N E, Radousky H B, Peng J L, Zhang L and Shelton R N 1990 *Physica* B **165–6** 1347
[34] Goodman G L 1990 unpublished results
[35] Maple M B, Ferreira J M, Hake R R, Lee B W, Neumeier J J, Seaman C L, Yang K N and Zhou H 1989 *J. Less-Common Met.* **149** 405
[36] Furukawa G T, Douglas T B and Pearlman N 1972 *American Institute of Physics Handbook* 3rd edn, ed D E Gray (New York: McGraw-Hill) sec 4e, pp 4-105–4-118
[37] See for example, Fast J D 1962 *Entropy* (New York: McGraw-Hill), particularly sec. 2.17 entitled Zero-point entropy and the 'third-law'